Full-Scale Characterization of UVLED $Al_xGa_{1-x}N$ Nanowires *via* Advanced Electron Microscopy

Patrick J. Phillips,[†,*] Santino D. Carnevale,[‡] Rajan Kumar,[§] Roberto C. Myers,[‡,⊥] and Robert F. Klie[†]

[†]Department of Physics, University of Illinois at Chicago, 845 West Taylor Street, Chicago, Illinois 60607, United States, [‡]Department of Materials Science and Engineering, Ohio State University, 2041 North College Road, Columbus, Ohio 43210, United States, [§]Department of Materials Science and Engineering, Northwestern University, 2220 Campus Drive, Evanston, Illinois 60208, United States, and [⊥]Department of Electrical and Computer Engineering, Ohio State University, 2015 Neil Avenue, Columbus, Ohio 43210, United States

ABSTRACT III-Nitride semiconductor heterostructures continue to attract a great deal of attention due to the wide range of wavelengths at which they can emit light, and the subsequent desire to employ them in optoelectronic applications. Recently, a new type of pn-junction which relies on polarization-induced doping has shown promise for use as an ultraviolet light emitting diode (UVLED); nanowire growth of this device has been successfully demonstrated. However, as these devices are still in their infancy, in order to more fully understand their physical and electronic properties, they require a multitude of characterization techniques. Specifically, the present contribution will discuss the application of advanced scanning transmission electron microscopy (STEM) to $Al_xGa_{1-x}N$ UVLED nanowires. In addition to structural data, chemical and electronic properties will also be probed through various spectroscopy techniques, with the focus remaining on practically applying the knowledge gained *via* STEM to the growth procedures in order to optimize device peformance.

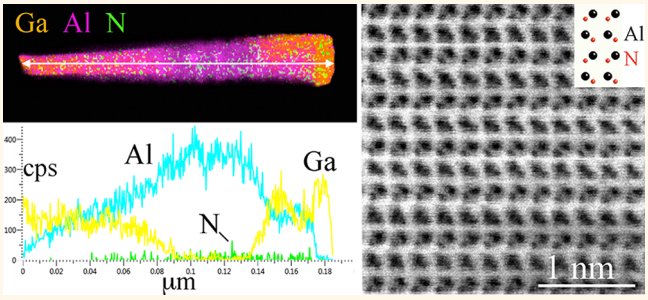

KEYWORDS: nitrides · nanowires · STEM · EDX · EELS

Because of the wide range of wavelengths at which they can emit light, there is great interest in III-N semiconductor heterostructures for use in optoelectronic applications.[1,2] However, the lack of a suitable substrate upon which to grow thin films leads to poor epitaxy and a subsequent high density of extended defects (*e.g.*, threading dislocations). In addition to cracking, these defects lead to states in the bandgaps and thus recombination centers and a loss of efficiency.[3] Nanowires are of particular interest to the GaN community as they effectively solve the "substrate issue" presented by conventional thin film growth. The large free-surface area of a nanowire allows the structure to effectively relax out much of the remnant strain, and thus, nanowires have become a viable solution to grow low-strain, defect-free III-N material; high quality $Al_xGa_{1-x}N$ structures have been repeatedly presented (see, for example, refs 4–6). Furthermore, due to their low defect concentration, more efficient photoluminescence has been demonstrated in nanowires as compared to planar structures.[2,7] It is important to note that, in addition to the structures being of higher quality, these wires can be grown on Si wafers, *i.e.*, commercially viable substrates.

Specifically, compositionally graded $Al_xGa_{1-x}N$ ultraviolet light emitting diode (UVLED) nanowires are the focus of the present contribution. The structures in question (first presented in Carnevale *et al.*[8]) are unique in that they do not rely on impurity doping, but rather on polarization-induced electron and hole doping.[9] First, a pn-junction is formed by grading a noncentrosymmetric crystal (such as GaN) from $x = 0$ to $x = 1$ and then back to $x = 0$. A GaN quantum well (QW) is then inserted into the center of the nanowire to increase the electron–hole recombination, and act as the active region for the device. Uniquely, these UVLEDs do not freeze-out at low

* Address correspondence to pjphil@uic.edu.

Received for review February 1, 2013 and accepted May 15, 2013.

Published online May 15, 2013
10.1021/nn4021407

temperatures, but still exhibit rectification and UV light emission at the bandgap, which can be tuned based on the composition and thickness of the QW.

As is often the case with nanofunctional materials, numerous characterization methods are required to drive the growth and fabrication processes forward, and electron microscopy continues to provide many desired capabilities. In particular, the scanning transmission electron microscope (STEM) fitted with a probe-side aberration corrector[10] yields unparalleled spatial resolution of both heavy and light chemical species. By including electron energy loss (EEL) and energy-dispersive X-ray (EDX) spectroscopies, one can complete a full-scale structural, chemical, and even electronic characterization of a wide range of relevant nanomaterials. In the present case, device efficiency is intimately linked with various physical properties at both the atomic and more macroscopic scales. For example, it is well-known that dislocations and other defects can act as recombination centers, reducing luminescent efficiency,[11] so basic structural characterization *via* high-resolution (HR) STEM imaging is necessary. Additionally, the active region's diameter, thickness, and residual strain are known to directly influence the structure's electronic properties, and as the material's bandgap will directly depend on its composition (3.4−6.2 eV in $Al_xGa_{1-x}N$), obtaining quantitative chemical data from the QW is required.[1,5,8,11,12] Moreover, it is imperative to verify the QW composition in order to confirm that the observed emission is indeed coming from the QW itself, and is not, for example, emission from a defect state. It is emphasized that the techniques presented below stand to benefit numerous electronic and photonic materials, including structures other than nanowires (*e.g.*, quantum dots and thin films) with compositions extending beyond Gallium and Aluminum.

As these nanowires are quite distinct from previous heterostructures, there exists a need to perform a full-scale characterization. All STEM-based methods were performed on a probe-corrected JEOL JEM-ARM200CF equipped with a cold field emission (CFEG) gun, operated at either 80 or 200 kV. The microscope is fitted with multiple detectors, including high and low angle annular dark field (HA/LAADF) and annular bright field (ABF). Capabilities exist to perform EELS and EDX characterization by way of a Gatan Enfina spectrometer and an Oxford X-Max80 silicon drift detector (SDD), respectively. Note that the only difference between the wires presented below and those described in Carnevale *et al.*[8] is the lack of an active region. Nevertheless, they serve as convenient structures to demonstrate the various characterization techniques available to the electronic materials community, and similar analyses to those presented here are subsequently underway on devices grown with an active region.

RESULTS AND DISCUSSION

HAADF and ABF images of a typical nanowire are presented in Figure 1a. General STEM imaging was performed at 200 kV, while EDX data was acquired at 80 kV, which yielded an improved count rate. The resolution at 200 and 80 kV is approximately 65 pm and 1.1 Å, respectively. Although not presented here, the ARM200CF is also capable of acquiring an LAADF image simultaneously with the HAADF/ABF pair. However, as these nanowires accommodate strain very well, there are no extended defects or other appreciable strain sources, so the LAADF image, which is sensitive to strain contrast,[13] reveals little new information and is not presented. Note that future devices may be grown with shorter graded regions or with QWs of varying thickness, both of which could lead to an increased strain; therefore, the LAADF information may prove to be quite useful. As the contrast in HAADF images is well-known to approach the square of the average atomic number (Z) of a given atomic column,[14−16] the extent of the Ga grading is readily visible as $Z_{Ga} = 31$, while $Z_{Al} = 13$. Figure 1b presents a higher magnification image of the graded region of a similar nanowire, with two stacking faults identified by arrows. Stacking faults have been repeatedly discussed in wurtzite structures and have been shown to affect electroluminescence properties of GaN;[17−19] thus, the importance of the seemingly rudimentary task of acquiring lattice images cannot be understated for these materials. The observation of stacking faults, although rare, in the present devices is particularly interesting, as it prompts a number of relevant materials science questions regarding their origin, *e.g.*, they could be strain-induced or a result of the compositional grading. Additionally, as the length of the graded region will affect the strain accommodation, this could prove to be another variable to explore in future device growth.

Following the more macroscopic structural characterization of Figure 1, chemical characterization techniques of both EDX and EEL spectroscopies were

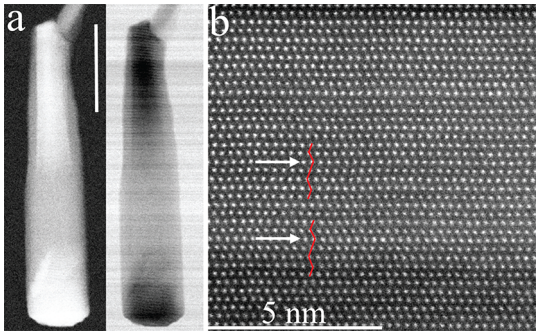

Figure 1. Overview of the structural characterization possible with STEM images: (a) HAADF/ABF images of a typical graded nanowire, scale bar is 50 nm; (b) HAADF image of a graded region containing multiple stacking faults; the normal stacking sequence as well as the disruption in stacking is indicated for each; arrows mark the faulted plane.

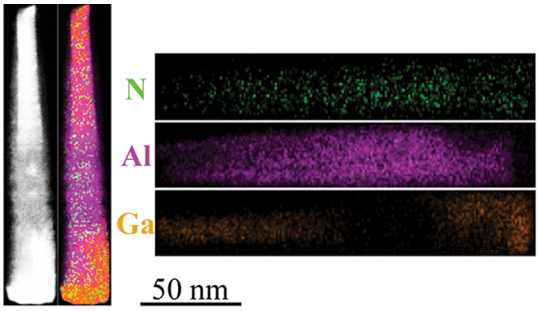

Figure 2. EDX results from a graded nanowire. HAADF signal and the HAADF signal with the Al, Ga, and N signals overlaid (binned twice) and raw data of the individual signals revealing a slight asymmetry at the wire top (image right) and a core–shell structure toward the wire bottom.

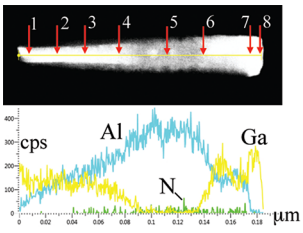

Spectrum	Ga / Al (at%)
1	58.4 / 41.6
2	52.2 / 47.8
3	29.6 / 70.4
4	18.6 / 81.4
5	0 / 100
6	10.8 / 89.2
7	69.4 / 30.6
8	100 / 0

Figure 3. EDX line scan results (left) and quantification of Al/Ga concentrations as a function of position along the wire.

employed. As heavy elements often have delayed-onset ionization edges which are difficult to characterize with EELS, compositional data is first acquired with EDX. The Ga and Al counts of Figure 2 confirm the targeted chemical gradation that was assumed based on the HAADF intensity. Furthermore, a line scan taken from the wire's approximate center is presented in Figure 3, along with several quantitative data sets taken from the areas indicated. Both the map and line scan reveal a slight radial asymmetry in the Ga gradation toward the top of the wire (at approximately 165 nm) that is not necessarily obvious given the HAADF image. The map also reveals the coaxial nature of AlN, most noticeably toward the bottom of the wire, where the GaN appears as a core to the shell of AlN. Thus, by coupling EDX and ABF imaging, the AlN shell can readily be characterized. In general, the active region should not be near any free surface of the device, as this can lead to surface recombination, so the AlN shell and its thickness and overall integrity will be relevant to device performance. Furthermore, this underscores the importance of being able to grow an active region which is entirely encased in a higher bandgap material (AlN), as discussed in Carnevale *et al.*[20] The individual spectra give quantitative confirmation of the targeted regions of either pure GaN or pure AlN at the wire top and bottom, respectively. Obviously, given the link between the active region's chemical makeup and the device's emission, similar chemical analyses can be performed in a systematic fashion on devices containing active regions with varying target compositions.

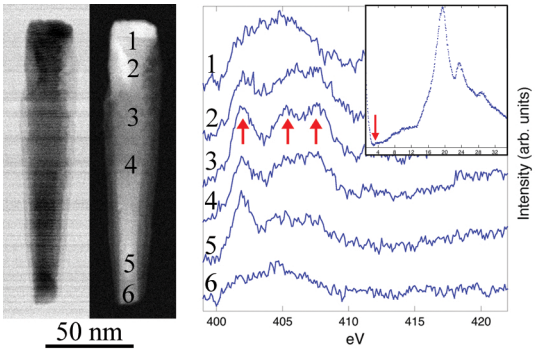

Figure 4. N K-edge EEL spectra as a function of position (and concentration) along a typical graded nanowire, acquired at 0.1 eV/pixel dispersion with a 5 s dwell time. Note that these spectra were extracted from a spectrum image (line scan) which was drift corrected every two pixels. All spectra were background subtracted with the usual power law assumption, but otherwise consist of raw data. Inset: Low-loss regime collected from a GaN reference demonstrating the capability of acquiring bandgap measurements; in this case, even in the raw data, there is a clear change in concavity at approximately 3.3–3.4 eV.

As one of the main goals of this type of characterization is compositional analysis as a function of position in the nanowire (and hence, growth parameters), it is beneficial to consider all possible avenues toward that goal, including EELS. For example, it has previously been demonstrated with X-ray absorption near-edge structure (XANES) that the Nitrogen K-edge is sensitive to x in $Al_xGa_{1-x}N$.[21,22] As illustrated in Figure 4, EELS analysis of the N K-edge can produce similar results. The background-subtracted N K-edge is presented as a function of position (thus, composition) across a graded nanowire. As demonstrated,[21] pure AlN will show three distinct peaks (spectrum #3) approximately 3 eV apart, while as x is decreased, the three peaks tend to agglomerate together to form a peak centered where the middle peak once was, with a slight shoulder where the left peak was. This is obvious in spectra #1 and #6, which are the most Ga-rich. However, in terms of resolving subtle shoulders, it is important to note that the previous XANES data was acquired with a resolution of approximately 0.1 eV, which is considerably better than most conventional STEM-EELS systems, and approximately equivalent to that achievable with monochromated STEM-EELS. Spectra #2, 4, and 5 then show some combination of GaN and AlN. Admittedly, spectrum #5 is a bit anomalous, as nowhere in the XANES data is the first peak the most intense. While this could be an indication of a preferential ordering near the base of the wire, it is interesting that this is also the region where the wire's core–shell structure is most apparent, both in the STEM images and EDX map. As discussed below in regards to polarity determination, ABF imaging, combined with multislice simulations, provides an avenue to probe such ordering effects. Lastly, no shifts in the edge onset energy are observed here, consistent with the XANES results.

An additional, somewhat obvious measurement to obtain is the material's bandgap. In particular, this measurement is critical to the present system because its continuous compositional gradation will alter the bandgap as a function of position along the nanowire. Again, this is a measurement made possible (without a monochromator) with the 0.35 eV resolution provided by the CFEG. The inset of Figure 4 presents a raw zero-loss spectrum from a reference film of pure GaN. The ability to measure various materials' bandgaps *via* low-loss EELS is a concept that has previously been demonstrated for systems like ZnO and InGaN nanowires, MgO cubes, GaN thin films, *etc.* (see, for example refs 23−26). It is important to note, however, that these measurements are often acquired on monochromated EELS systems. In the present case, the obvious extension of this type of analysis is to acquire position-sensitive bandgap measurements along the nanowires' graded regions, and from within their active regions.

Beyond compositional effects, it is important to realize that EELS can be used to probe a material's density of states and is therefore an efficient method to investigate electronic structure, which is ultimately linked to efficiency in the $Al_xGa_{1-x}N$ UVLEDs.[27] For example, previous work on dislocations in GaN demonstrated a change in the EELS N K-edge fine structure with the probe placed over a bulk region of crystal compared to over a defect. In addition to noting Oxygen segregation (and corresponding Nitrogen depletion), by analyzing the N K-edge, localized states were identified in the band gap due to Oxygen.[28,29] This is particularly relevant to the current system because Al is an O-getter, and hence, there is believed to be a nominal Oxygen concentration present; EELS will therefore provide a route to quantify any effects of O-defects on the electronic structure, and hence device efficiency.

A given nanowire's structural properties can be probed *via* large-scale STEM imaging and EDX mapping, while defect identification is possible through HR HAADF STEM. Electronic properties, on the other hand, can be fleshed out of both perfect and defected regions with local (position sensitive) EELS fine structure (N K-edge) and low loss (bandgap) analyses. However, certain findings, such as the potential ordering identified by the EELS N K-edge data above, require either a multifaceted approach or a different technique altogether. In this case, we turn to simultaneous high resolution HAADF/ABF STEM imaging, such as that presented in Figure 5, in conjunction with multislice image simulations (Figure 6). Annular bright field images have recently drawn much attention due to their sensitivity to light elements, yet resiliency to conventional phase-contrast interpretability issues with changing defocus and specimen thickness.[30] In general, Nitrogen is clearly observable in the ABF image, although it is

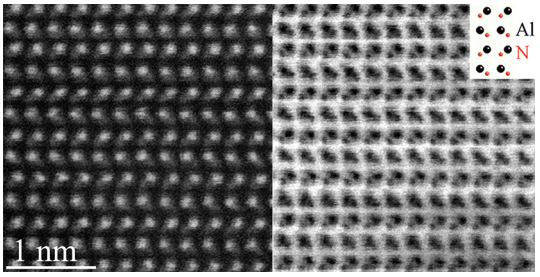

Figure 5. HAADF/ABF pair of images of a region which should be largely AlN. Note the N visibility in the ABF image and the tails of intensity where the N would be in the HAADF image.

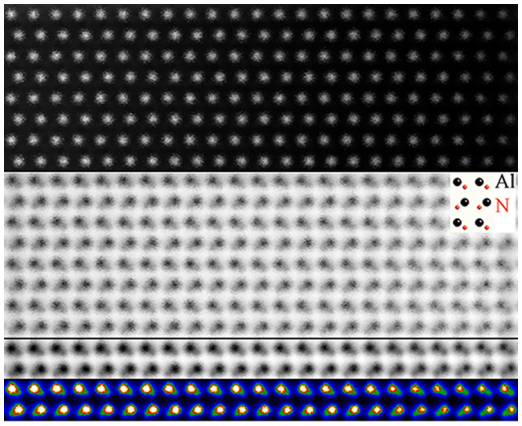

Figure 6. Multislice results (HAADF/ABF) from a compositionally graded input cell taken at the crystal's full thickness: 19.8 nm. Moving left to right, the composition grades from pure GaN to pure AlN. The two bottom strips are the same cross-correlated and vertically averaged image, one grey-scale (upper) and one in false-color (lower), with the latter highlighting the N visibility as green; see text for details.

interesting to note that it appears to be more readily identifiable in approximately every-other lattice plane; this could be a direct visualization of Al-rich or Ga-rich lattice planes. Given the relative sizes and scattering strengths of the atoms in question (N, Al, and Ga), it is possible that the weakly scattering N signal is blurred out by the Ga signal in Ga-rich regions. If indeed this does demonstrate subtle Ga penetration into otherwise Al-dominant columns, it is certainly reasonable that the Ga intensity simply dominates the HAADF signal, whereas the Al signal will not do so, thus allowing for the N tails to be more easily seen in regions of AlN.

Multislice STEM image simulations[31] were carried out in order to further probe the possibility of compositional fluctuations affecting N-column visibility in the ABF mode, with results presented in Figure 6. Specifically, the simulated crystal is 19.8 nm thick; the composition in the image plane grades from GaN (left) to AlN (right) and does not vary in the vertical direction. Clearly, the visibility of N-columns is affected by the crystal either being GaN- or AlN-rich, as Nitrogen is more readily visible on the righthand side of the simulated image and the Al−N show more separation than the

larger Ga atoms bonded to N. Since there is no compositional variation in the vertical direction, the N-column visibility is more clearly observed in the subimage of Figure 6, which resulted from the full image having been divided into strips two atomic rows wide, then cross-correlating and averaging those strips down the image vertical. This method will prove to be useful in future efforts toward validating compositional effects on ABF images, particularly those obtained within a QW where there will be some targeted composition of $Al_xGa_{1-x}N$. Indeed, it is through this approach combining multiple scales of imaging and chemical analysis with computational results that a full-scale analysis can be performed on structures such as these nanowires.

As perhaps the most important benefit of ABF STEM, the direct imaging of Nitrogen allows one to determine the polarity of the nanowire, which will determine the carrier type in the graded section, therefore the diode orientation, and thus directly influence the device's properties. In the case of GaN or AlN, polarization is characterized by the direction of the "long" Ga−N or Al−N bond that is colinear with the crystal's *c*-axis, and hence is the polarity is directly characterized from an atomic-resolution ABF image.[32,33] In the present analysis, one of the more pertinent results was discovering a large fraction of the wires to be of N-face orientation, despite being optimized for Ga-face polarity. Subsequent electroluminescence measurements on, for example, an ensemble of nanowires connected in parallel demonstrated that wires with opposite polarity will emit light under opposite biases, with a greater emission intensity resulting from N-face wires being "turned on" (Carnevale, *et al.*, private communication). While much more detail will be available in a forthcoming publication, the importance of understanding the nanowires' mixed polarity is nevertheless underscored, along with the iterative nature of device growth and characterization which is often necessary with new structures. Specifically, as a direct result of the ABF STEM investigation, new device designs optimized for N-face orientation are now underway.

CONCLUSIONS

In short, it is apparent that modern probe-corrected STEM instruments can provide sufficient tools to perform a full-scale study of various nanomaterials, such as $Al_xGa_{1-x}N$ UVLED nanowires, in order to drive device development by linking physical characteristics to device properties. It is important to realize that the characterization methods reported here are applicable to a wide range of relevant materials in the community, including—but not limited to—nanowires, thin films, and quantum structures. The full suite of tools provided by electron microscopy is an important requirement to address a wide range of nanoscale characterization questions. For example, in the present case, image simulations revealed some Ga atoms present within a largely AlN region, yielding anomalous ABF STEM images, while N K-edge EELS data identified regions of the nanowire which are electronically varied, potentially due to either the wire's core−shell nature, or the presence of defects. With these and the other techniques presented above, the door is certainly open to combine multiple characterization techniques, spanning multiple length scales and chemical signals, to continue to drive the efficiency and functionality of nanomaterials.

METHODS

General STEM imaging was performed at 200 kV with a convergence angle of 22 mrad and a probe current of 10.5 pA. A spatial resolution of approximately 65 pm can be realized with the microscope in this configuration, while just under 80 pm is a routinely attainable value. The HAADF inner detection angle was set to 90 mrad, which yields an ABF inner detection angle of approximately one-half the convergence angle, which is common practice.[34] To extract the nanowires for STEM observations, a carbon-coated Cu grid was simply rubbed over the surface of the as-grown sample, which consisted of vertically oriented nanowires on a silicon substrate. To avoid projection artifacts, all wires were tilted to a low index zone axis with the *c*-axis perpendicular to the incident beam for both imaging and chemical analysis. For chemical mapping, the convergence angle is often expanded by 33% and the probe current is increased by a factor of 30; the resolution in this configuration remains sub-Å. In general, to fully reap the benefits of the CFEG in terms of EELS energy resolution, the HR-STEM probe is modified by decreasing the tip emission current to 0.5−1 μA. With the modified EELS probe, an energy resolution of 0.35 eV is possible, while the spatial resolution remains at approximately 1.1 Å. To yield an improved count rate, EDX data was acquired at 80 kV, which provided a sufficient spatial resolution of $\approx$1.2 Å.[35]

Regarding the EDX data, note that the two areas of increased intensity within the AlN slab are not chemical in nature, but are small regions of contamination resulting from focusing and stigmating on the crystal at a high magnification. Since the nanowire itself is the only feature in a zone axis orientation during a given experiment, one is forced to do such fine alignments on the structure; even working quickly can cause contamination. Additionally, since the nanowires are supported on a carbon film, the typical preparatory step of plasma cleaning cannot reasonably be performed; a beam shower is generally a sufficient substitute. The EDX data sets presented in Figure 3 came from the map of Figure 2, post acquisition, simply by placing user-defined regions (boxes approximately 5−8 nm per side) over an area of interest; the spectra contained within that area are then summed. The quantitative analysis yielded weight % Sigma values between 2 and 5. It is noted that this is simply a statistical uncertainty, and does not account for auxiliary effects, for example specimen geometry. Considering, however, that the scans were acquired in the center of a thin, cylindrical object, we do not anticipate EDX artifacts arising from thicker specimens with more complicated geometries (*e.g.*, wedge-shaped). For some regions of interest, the N-signal was not sufficient for quantification, so only Al and Ga were quantified. Thus, the results are listed as atomic percentages, assuming the structure contains only two species: Al and Ga. For spectra that did contain quantifiable N, this is equivalent to adding the atomic percent N contributed to either GaN or AlN in proportion to the percent of Ga or Al identified. In essence, the numbers presented in Figure 3 can be thought of as the atomic percentages of GaN and AlN. Note that Cu and C signals were omitted from the quantitative spectra.

Multislice simulations have been demonstrated to be a valid and efficient means to perform atomic-scale calculations.[14,36] The multislice algorithm converts a thick specimen into thin slices, calculates the projected atomic potential for each slice, then allows for alternating transmittance and propagation of the electron wave function throughout the total specimen thickness. The present simulations employ the "frozen phonon" approximation, which successfully introduces thermal vibrations into multislice calculations.[15,31,37,38] The input supercell was created such that it is graded through its depth from pure AlN to pure GaN. In other words, if the imaging direction is taken as parallel to [001], the crystal is pure GaN below a line parallel to the ($\bar{1}$01) plane and pure AlN above it. Therefore, the composition in the image plane grades from GaN (left) to AlN (right) and does not vary in the vertical direction.

Conflict of Interest: The authors declare no competing financial interest.

Acknowledgment. P.J.P. is grateful to N. Rowlands of Oxford and K.-B. Low and A. Nicholls of the UIC Research Resources Center. The UIC JEOL JEM-ARM 200CF is supported by an MRI-R^2 grant from the National Science Foundation (Grant No. DMR-0959470).

REFERENCES AND NOTES

1. Armitage, R.; Tsubaki, K. Multicolor Luminescence from InGaN Quantum Wells Grown over GaN Nanowire Arrays by Molecular-Beam Epitaxy. *Nanotechnology* **2010**, *21*, 195202.
2. Li, S.; Waag, A. GaN Based Nanorods for Solid State Lighting. *J. App. Phys* **2012**, *111*, 071101.
3. Park, Y. S.; Lee, S.-H.; Oh, J.-E.; Park, C.-M.; Kang, T.-W. Self-Assembled GaN Nano-Rods Grown Directly on (111) Si Substrates: Dependence on Growth Conditions. *J. Cryst. Growth* **2005**, *282*, 313–319.
4. Bertness, K. A.; Sanford, N. A.; Davydov, A. V. GaN Nanowires Grown by Molecular Beam Epitaxy. *IEEE J. Sel. Top. Quantum Electron.* **2011**, *17*, 847–858.
5. Rigutti, L.; Tchernycheva, M.; De Luna Bugallo, A.; Jacopin, G.; Julien, F. H.; Zagonel, L. F.; March, K.; Stephan, O.; Kociak, M.; Songmuang, R. Ultraviolet Photodetector Based on GaN/AlN Quantum Disks in a Single Nanowire. *Nano Lett.* **2010**, *10*, 2939–2943.
6. Carnevale, S. D.; Marginean, C.; Phillips, P. J.; Kent, T. F.; Sarwar, A. T. M. G.; Mills, M. J.; Myers, R. C. Coaxial Nanowire Resonant Tunneling Diodes from Non-Polar AlN/GaN on Silicon. *App. Phys. Lett.* **2012**, *100*, 142115.
7. Bertness, K. A.; Sanford, N. A.; Barker, J. M.; Schlager, J. B.; Roshko, A.; Davydov, A. V.; Levin, I. Catalyst-Free Growth of GaN Nanowires. *J. Electron. Mater.* **2006**, *35*, 576–580.
8. Carnevale, S. D.; Kent, T. F.; Phillips, P. J.; Mills, M. J.; Rajan, S.; Myers, R. C. Polarization-Induced pn Diodes in Wide-Band-Gap Nanowires with Ultraviolet Electroluminescence. *Nano Lett.* **2012**, *12*, 915–920.
9. Simon, J.; Protasenko, V.; Lian, C.; Xing, H.; Jena, D. Polarization-Induced Hole Doping in Wide-Band-Gap Uniaxial Semiconductor Heterostructures. *Science* **2010**, *327*, 60–64.
10. Haider, M.; Rose, M.; Uhlemann, S.; Schwan, E.; Kabius, B.; Urban, K. A Spherical-Aberration-Corrected 200 kV Transmission Electron Microscope. *Ultramicroscopy* **1998**, *75*, 53–60.
11. Sekiguchi, H.; Kato, K.; Tanaka, J.; Kikuchi, A.; Kishino, K. Ultraviolet GaN-Based Nanocolumn Light-Emitting Diodes Grown on n-(111) Si Substrates by rf Plasma-Assisted Molecular Beam Epitaxy. *Phys. Status Solidi A* **2008**, *205*, 1067–1069.
12. Shur, M. S.; Gaska, R. Deep-Ultraviolet Light-Emitting Diodes. *IEEE Trans. Electron Devices* **2010**, *57*, 12–25.
13. Phillips, P. J.; De Graef, M.; Kovarik, L.; Agrawal, A.; Windl, W.; Mills, M. J. Atomic-Resolution Defect Contrast in Low Angle Annular Dark-Field STEM. *Ultramicroscopy* **2012**, *116*, 47–55.
14. Kirkland, E. J.; Loane, R. F.; Silcox, J. Simulation of Annular Dark Field STEM Images Using a Modified Multislice Method. *Ultramicroscopy* **1987**, *23*, 77–96.
15. Loane, R.; Xu, P.; Silcox, J. Incoherent Imaging of Zone Axis Crystals with ADF STEM. *Ultramicroscopy* **1992**, *40*, 121–138.
16. Treacy, M. Optimising Atomic Number Contrast in Annular Dark Field Images of Thin Films in the Scanning Transmission Electron Microscope. *J. Microsc. Spectrosc. Electron.* **1982**, *7*, 511–523.
17. Khromov, S.; Hemmingsson, C. G.; Amano, H.; Monemar, B.; Hultman, L.; Pozina, G. Luminescence Related to High Density of Mg-Induced Stacking Faults in Homoepitaxially Grown GaN. *Phys. Rev. B* **2011**, *84*, 075324.
18. Stampfl, C.; Van de Walle, C. G. Energetics and Electronic Structure of Stacking Faults in AlN, GaN, and InN. *Phys. Rev. B* **1998**, *57*), 052–055.
19. Tham, D.; Nam, C.-Y.; Fischer, J. E. Defects in GaN Nanowires. *Adv. Funct. Mater.* **2006**, *16*, 1197–1202.
20. Carnevale, S. D.; Yang, J.; Phillips, P. J.; Mills, M. J.; Myers, R. C. Three-Dimensional GaN/AlN Nanowire Heterostructures by Separating Nucleation and Growth Processes. *Nano Lett.* **2011**, *11*, 866–871.
21. Duda, L. C.; Stagarescu, C. B.; Downes, J.; Smith, K. E.; Korakakis, D.; Moustakas, T. D.; Guo, J.; Nordgren, J. Density of States, Hybridization, and Band-Gap Evolution in $Al_xGa_{1-x}N$ Alloys. *Phys. Rev. B* **1998**, *58*, 1928–1933.
22. Keast, V. J.; Scott, A. J.; Brydson, R.; Williams, D. B.; Bruley, J. Electron Energy-Loss Near-Edge structure - a Tool for the Investigation of Electron Structure on the Nanometre Scale. *J. Microsc.* **2001**, *203*, 135–175.
23. Lazar, S.; Botton, G. A.; Wu, M.-Y.; Tichelaar, F. D.; Zandbergen, H. W. Materials Science Applications of HREELS in Near Edge Structure and Low-Energy Loss Spectroscopy. *Ultramicroscopy* **2003**, *96*, 535–546.
24. Wang, J.; Li, Q.; Egerton, R. Probing the Electronic Structure of ZnO Nanowires by Valence Electron Energy Loss Spectroscopy. *Micron* **2007**, *38*, 346–353.
25. Kuykendall, T.; Ulrich, P.; Aloni, S.; Yang, P. Complete Composition Tunability of InGaN Nanowires Using a Combinatorial Approach. *Nat. Mater.* **2007**, *6*, 951–956.
26. Rafferty, B.; Pennycook, S. J.; Brown, L. M. Zero Loss Peak Deconvolution for Bandgap EEL Spectra. *J. Electron Microsc.* **2007**, *49*, 517–524.
27. Tricker, D. M.; Natusch, M. K. H.; Boothroyd, C. B.; Xin, Y.; Brown, P. D.; Cheng, T. S.; Foxon, C. T.; Humphreys, C. J. Probing the Effect of Defects on Band Structure in GaN. *Inst. Phys. Conf. Ser.* **1997**, 217–220.
28. Arslan, I.; Browning, N. Role of Oxygen at Screw Dislocations in GaN. *Phys. Rev. Lett.* **2003**, *91*, 165501.
29. Arslan, I.; Bleloch, A.; Stach, E. A.; Ogut, S.; Browning, N. Using EELS to Observe Composition and Electronic Structure Variations at Dislocation Cores in GaN. *Philos. Mag.* **2006**, *86*, 4727–4746.
30. Findlay, S. D.; Shibata, N.; Sawada, H.; Okunishi, E.; Kondo, Y.; Ikuhara, Y. Dynamics of Annular Bright Field Imaging in Scanning Transmission Electron Microscopy. *Ultramicroscopy* **2010**, *110*, 903–923.
31. Kirkland, E. J. *Advanced Computing in Electron Microscopy*, 2nd ed.; Springer: New York, 2010.
32. de la Mata, M.; Magen, C.; Gazquez, J.; Utama, M. I. B.; Heiss, M.; Lopatin, S.; Furtmayr, F.; Fernández-Rojas, C.; Peng, B.; Morante, J. R.; *et al.* Polarity Assignment in ZnTe, GaAs, ZnO, and GaN-AlN Nanowires from Direct Dumbbell Analysis. *Nano Lett.* **2012**, *12*, 2579–2586.
33. Hestroffer, K.; Leclere, C.; Bougerol, C.; Renevier, H.; Daudin, B. Polarity of GaN Nanowires Grown by Plasma-Assisted Molecular Beam Epitaxy on Si(111). *Phys. Rev. B* **2011**, *84*, 245301.
34. Findlay, S. D.; Shibata, N.; Sawada, H.; Okunishi, E.; Kondo, Y.; Yamamoto, T.; Ikuhara, Y. Robust Atomic Resolution Imaging of Light Elements Using Scanning Transmission Electron Microscopy. *App. Phys. Lett.* **2009**, *95*, 191913.
35. Qiao, Q.; Klie, R. F.; Öğüt, S.; Idrobo, J. C. Atomic and Electronic Structures of $SrTiO_3$/GaAs Heterointerfaces: An 80-kV Atomic-Resolution Electron Energy-Loss Spectroscopy Study. *Phys. Rev. B* **2012**, *85*, 165406.

36. Loane, R.; Kirkland, E.; Silcox, J. Visibility of Single Heavy Atoms on Thin Crystalline Silicon in Simulated Annular Dark-Field STEM Images. *Acta Crystallogr.* **1988**, *A44*, 912–927.
37. Hillyard, S.; Silcox, J. Detector Geometry, Thermal Diffuse Scattering, and Strain Effects in ADF STEM Imaging. *Ultramicroscopy* **1995**, *58*, 6–17.
38. Silcox, J.; Xu, P.; Loane, R. Resolution Limits in Annular Dark Field STEM. *Ultramicroscopy* **1992**, *47*, 173–186.